5-1-2020

Characterization of Adnexal Masses Using Contrast-Enhanced Subharmonic Imaging: A Pilot Study.

Lauren J. Delaney
Thomas Jefferson University

Priscilla Machado
Thomas Jefferson University

Mehnoosh Torkzaban
Thomas Jefferson University

Andrej Lyshchik
Thomas Jefferson University

Corinne Wessner
Thomas Jefferson University

Authors

Lauren J. Delaney; Priscilla Machado; Mehnoosh Torkzaban; Andrej Lyshchik; Corinne Wessner; Christine H. Kim, MD; Norman G Rosenblum; Scott D. Richard; Kirk Wallace; and Flemming Forsberg

Characterization of Adnexal Masses Using Contrast-Enhanced Subharmonic Imaging: A Pilot Study

Lauren J. Delaney [a], Priscilla Machado [a], Mehnoosh Torkzaban [a], Andrej Lyshchik [a], Corinne E. Wessner [a], Christine Kim [b], Norman Rosenblum [b], Scott Richard [b], Kirk Wallace [c], Flemming Forsberg [a]

[a] Department of Radiology, Thomas Jefferson University, Philadelphia, PA 19107, USA

[b] Division of Gynecologic Oncology, Thomas Jefferson University, Philadelphia, PA 19107, USA

[c] GE Global Research, Niskayuna, NY 12309, USA

Corresponding Author:

Flemming Forsberg, PhD

Department of Radiology

Thomas Jefferson University

132 S. 10th Street, Main 763

Philadelphia, PA 19107

Phone: (215) 955-4870

Email: flemming.forsberg@jefferson.edu

Abstract

This pilot study evaluated whether contrast-enhanced subharmonic imaging (SHI) could be used to characterize adnexal masses prior to surgical intervention. Ten women (with 12 lesions) scheduled for surgery of an ovarian mass underwent a SHI examination of their adnexal region using a modified Logiq E9 scanner (GE, Waukesha, WI) with an endocavitary probe, where digital clips were acquired using pulse destruction/replenishment SHI imaging across the lesion. Time intensity curves were created off-line to quantitatively evaluate SHI parameters (fractional tumor perfusion, peak contrast intensity, time to peak contrast enhancement, and area under the time intensity curve), which were compared to pathological characterization of the lesion. Of the 12 masses, 8 were benign and 4 were malignant. Qualitative analysis of the SHI images by an experienced radiologist resulted in a diagnostic accuracy of 70%, compared to 56% without contrast, while an inexperienced radiologist improved from 50% to 58% accuracy, demonstrating the benefit of SHI. Quantitative analysis of SHI parameters produced diagnostic accuracy as high as 81%. Peak contrast intensity was significantly greater in malignant than benign masses (0.109 ± 0.088 AU vs. 0.046 ± 0.030 AU, $p = 0.046$). Malignant masses also demonstrated significantly greater perfusion than benign masses (24.79 ± 25.34% vs. 7.62 ± 6.50%, $p = 0.045$). When the radiologist reads were combined with the most predictive quantitative SHI parameter (% perfusion), diagnostic accuracy improves to 84% for the experienced radiologist and 96% for the novice radiologist. Results indicate SHI for pre-surgical characterization of adnexal masses may improve the determination of malignancy and diagnostic accuracy; albeit based on a small sample size.

Keywords:

Subharmonic imaging, adnexal masses, diagnostics, contrast agents

Introduction

Ovarian cancer is the seventh most commonly diagnosed cancer in women worldwide, with approximately 240,000 new cases diagnosed and 152,000 deaths each year (representing a 64% mortality rate) [1]. Ovarian cancer is also the fifth most common cause of cancer death in women in the United States, and an estimated 1 in 71 women in the United States will develop ovarian cancer in their lifetime [2, 3]. If caught early enough that disease is confined to the ovary (stage I), patients require less morbid surgical intervention, have significantly improved quality of life, and most importantly have a 5-year survival rate of approximately 90% [2, 4, 5]. Unfortunately, roughly 75% of new diagnoses are late-stage cancers, bringing the mortality rates up as high as 80% [5]. The prevalence of late-stage diagnoses clearly highlights the inadequacy of conventional endovaginal ultrasound (US) imaging and pelvic examinations as the first-line in detecting adnexal masses [6-8]. Additionally, once detected, many adnexal masses are deemed clinically indeterminate with first-line US imaging, and follow-up magnetic resonance (MR), and computerized tomography (CT) imaging cannot always definitively characterize them as benign or malignant [9, 10]. Therefore, up to 80% of presenting patients undergo surgery out of an abundance of caution, in response to the aforementioned mortality rates for late-stage disease [11-13]. Thus, there is a clear clinical need for earlier and accurate characterization of adnexal masses to improve patient survival.

Imaging techniques can play a critical role in improving detection and diagnosis of ovarian masses, especially in the assessment of angiogenesis and blood perfusion in the lesion [6, 7, 14, 15]. One of the earliest changes that differentiates cancerous tissues from

normal tissues is tumor angiogenesis [16, 17]. Additionally, the morphology of these angiogenic vessels can serve as a predictor of malignancy in cancerous masses [18, 19], including those in the adnexal region [20, 21]. Angiogenic vessels form a substantial portion of the mass of malignant lesions (up to 10% of total tumor volume) [22], providing a strong opportunity for noninvasive imaging to improve on the classification of these adnexal lesions compared to purely anatomical imaging modes. While contrast-enhanced MR and CT can be up to 90% accurate in classifying adnexal masses that were deemed indeterminate with first-line US [6, 23], these secondary modalities are costly and utilize contrast agents associated with marked adverse reactions, and CT also exposes patients to significant ionizing radiation. However, contrast-enhanced US (CEUS) imaging has great potential to provide clinically relevant information related to measuring angiogenesis and blood flow in adnexal lesions. Specifically, CEUS imaging using gas microbubbles greatly improves the ability to visualize tumor angiogenesis and quantify blood flow within tumors, including adnexal masses, without the marked adverse reactions and contraindications of MR and CT contrast [14, 24-26]. Several studies have shown that CEUS imaging can be useful in classification of adnexal masses as benign or malignant [14, 26-29], and characterizing blood flow kinetics in these masses [30]. However, these techniques fall short of clinically viable accuracy in diagnosis, likely due to image degradation and reduction in blood-to-tissue contrast in tissue [31].

In an effort to address this clinical need, we have been developing a contrast-specific imaging modality known as subharmonic imaging (SHI). SHI transmits the ultrasound signal at twice the resonance frequency ($2f_0$) of the ultrasound contrast agent (UCA) and receives at half of the transmit frequency (f_0), which allows for excellent

suppression of tissue echoes relative to other US contrast modes [32, 33]. Although other modes, such as contrast pulse sequences (CPS), pulse inversion, and flash-replenishment, can be used for tissue suppression, SHI combines the ability to specifically suppress tissue echoes while also providing quantitative data. Our group, as well as others, have performed extensive SHI feasibility studies [25, 34-47]. We have also demonstrated that SHI can detect the slow, small volume blood flow associated with tumor angiogenesis in a first-in-humans study of women with breast lesions [34, 40-42]. Moreover, UCAs are pure intravascular tracers and enable CEUS to depict tumor vascularity differently from MR, which uses gadolinium chelates as contrast agents. Given these advantages, CEUS utilizing SHI could help address the critical clinical need by providing a more accurate imaging technique at earlier stages, and may ultimately improve patient survival. Therefore, the objective of this pilot study was to evaluate whether contrast-enhanced SHI could help characterize adnexal masses prior to surgical intervention.

Materials and Methods

Patient Recruitment and Clinical Pathology

Twenty-eight women scheduled for surgery of suspicious ovarian lesions at Thomas Jefferson University between August 2017 and August 2018 who met the inclusion criteria for this IRB-approved study were approached to participate. Twelve women agreed to enroll, and signed informed consent to participate in the study and undergo a contrast-enhanced SHI exam of the adnexal region prior to surgery. Two women declined to participate and withdrew consent prior to contrast administration, for

a total of ten participants who completed the study. Inclusion criteria included diagnosis with an adnexal mass, plan for surgical resection of adnexal mass, at least 21 years of age, and clinically stable. Pre-menopausal subjects had to have a negative pregnancy test to be enrolled in the study, since pregnancy was one of the exclusion criteria for study participation. Other exclusion criteria included pulmonary hypertension, cardiac shunts, or unstable cardiopulmonary conditions, current systemic chemotherapy regimen, clinical instability or terminal illness with a life expectancy of less than 1 month, and history of anaphylactic allergy to ultrasound contrast agents. Study subjects ranged in age from 34 to 76 years old, with an average age of 55.5 years. Tumor marker CA-125 and risk of malignancy (RMI) were determined by pathological evaluation. Following surgery, excised lesions were classified by clinical pathology as part of standard of care.

Contrast-Enhanced SHI Evaluation

Contrast-enhanced SHI scanning was performed using a Logiq E9 scanner (GE Healthcare, Waukesha, WI) equipped with an IC5-9-D endocavitary probe, using three pulse coded excitation SHI mode with a transmit frequency of 7.0 MHz and receiving at 3.5 MHz. Using coded excitation will have marked improvements in signal-to-noise ratio, due to suppression of tissue signals [48]. Imaging was optimized on an individual basis, using a mechanical index (MI) below 0.18 in all cases (ranged from 0.10 – 0.18, average 0.13). Patients first received a 1.5 mL intravenous bolus injection of Definity® (Lantheus Medical Imaging, N Billerica, MA), while digital clips of the lesion in the area with the most flow seen using power Doppler were acquired for up to 5 minutes after injection. Patients then rested for 10 minutes to ensure contrast clearance before receiving an infusion of 1.5 mL of Definity diluted in 25 mL of sterile saline over 5 minutes, where digital clips were

acquired during flash-replenishment SHI imaging across the lesion, including the same areas that were previously imaged. These sequences consisted of destructive US pulses at an average mechanical index (MI) of 0.6 (ranged from 0.5 – 0.8), which ruptured the UCA within the imaging plane, followed by nonlinear SHI imaging at a lower intensity (MI of 0.07) to allow monitoring of the UCA re-perfusion into the lesion. An average of 6 pulses per lesion were collected, with at least 4 per lesion, as the number of pulses collected was subjective on a case-by-case basis.

Time-intensity curves (TICs) and parametric maps were generated offline using Matlab (MathWorks, Natick, MA) to quantitatively evaluate SHI parameters from the flash-replenishment sequences. These curves estimate perfusion over the adnexal lesion by calculating the slope of the curve from the time contrast was first visualized to the peak intensity. Data from TICs were used to calculate estimated fractional tumor perfusion (PER), peak contrast intensity (PI), area under the TIC (AUC), and time to peak contrast enhancement (TTP), which is defined as the time from contrast infusion to the point at which maximum pixel intensity is reached [25, 40]. The TIC was also fit with a two-parameter exponential recovery curve: $VI = \alpha(1 - e^{-\beta t})$, in which VI represents video intensity, α (dB) represents the asymptotic plateau correlative of the microvessel cross-sectional area, and β (mm/s) represents the blood velocity [49-51]. The product α x β is an estimate of perfusion or blood flow per tissue unit (mL/(s*mg)).

Additionally, qualitative assessment of the SHI images was performed by two radiologists, one who was experienced with CEUS (more than 10 years of experience) and one who was not (around 6 months of experience). The radiologists were blinded to the pathological classification of the lesions, and were given both grayscale and contrast-

enhanced SHI clips for evaluation. After reviewing each case, the radiologists provided a qualitative score for diagnosis based purely on their assessment of the images using a 5-point visual analog scale, with 1 representing benign and 5 malignant, and their confidence in that diagnosis (on a percent scale).

Statistical Analysis

Statistical analysis was performed with Stata 15 (StataCorp, College Station, TX), using t-tests ($\alpha < 0.05$) to compare the data between response groups. Receiver operating characteristics (ROC) curves were used to determine diagnostic accuracies as the area under the ROC curve [52]. Reverse stepwise logistical regression was used to combine qualitative and quantitative results to test for improved accuracy. Results were collected in triplicate, and error is reported as standard deviation (SD).

Results

Clinical Evaluation of Adnexal Masses

Two patients withdrew their consent and did not complete the study, while ten patients completed their ultrasound scans. Of these ten patients, two had two adnexal lesions; for a total of 12 lesions analyzed in this study. Clinical pathology determined that 8 (67%) of the lesions were benign and 4 (33%) were malignant. Benign lesions were classified as mucinous cystadenoma (3), hydrosalpinx (2), mature cystic teratoma (1), mixed epithelial neoplasm (1), and endometriosis (1). Malignant lesions were classified as carcinosarcoma (2), serous adenocarcinoma (1), and adenocarcinoma from colonic metastasis (1). In the two patients presenting with two lesions, the pathological finding was consistent for both lesions (i.e. both were benign or both were malignant). Tumor

marker CA-125 and risk of malignancy index (RMI) were collected for 8 of the 12 lesions, including 5 of the 8 classified as benign and 3 of the 4 classified as malignant. CA-125 levels in benign lesions (17.46 ± 8.42 nL) were statistically similar to levels in malignant lesions (56.20 ± 75.17 nL, $p = 0.27$). CA-125 had a diagnostic accuracy of 60% in this pilot study. There was also no statistical difference in the RMI between benign and malignant lesions (104.00 ± 95.67 vs. 505.67 ± 676.65, $p = 0.22$). The diagnostic accuracy for RMI was 73%.

Quantitative Analysis of Contrast-Enhanced SHI

Representative images of lesions classified as malignant and benign are shown in Figure 1. Malignant lesions (Figs. 1A and C) typically presented with hyperechoic regions that demonstrated increased blood flow on SHI, while benign lesions (Figs. 1B and D) typically presented with hypoechoic and/or anechoic regions that indicated fluid-filled cysts.

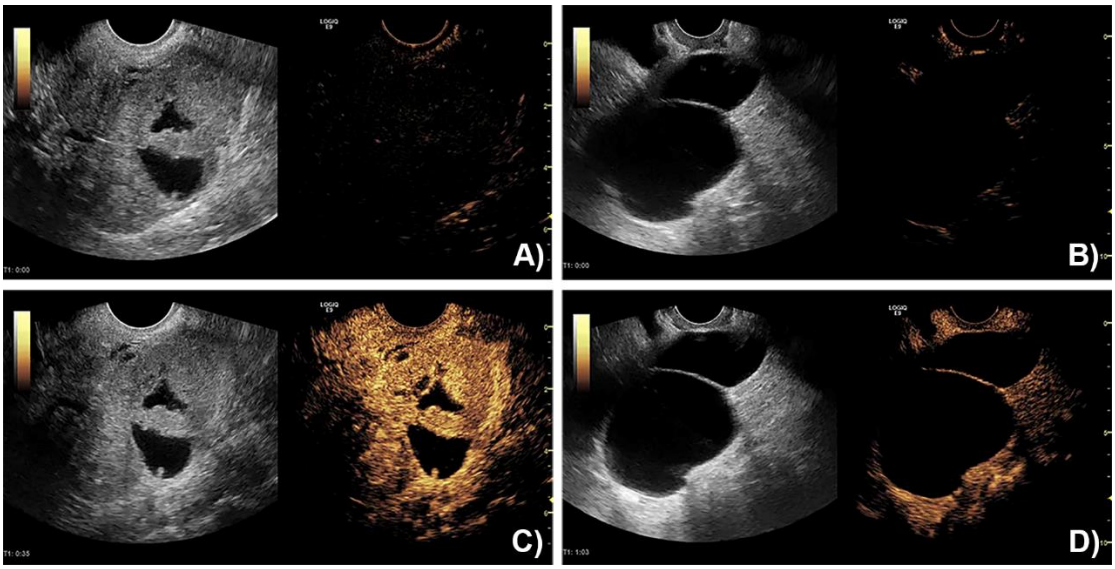

Figure 1: Representative SHI images from study patients. A) Pre-contrast image of a lesion later classified as malignant by pathology. B) Pre-contrast image of a lesion later classified as benign by pathology. C) SHI of the malignant lesion shown in panel A. D) SHI of the benign lesion shown in panel B.

The outcomes of the quantitative SHI analysis are summarized in Table 1, and representative time-intensity curves are shown in Figure 2. Peak contrast intensity (PI) was significantly greater in malignant than benign masses (0.109 ± 0.088 vs. 0.046 ± 0.030, $p = 0.046$). Malignant masses also demonstrated significantly greater PER than benign masses (24.79 ± 25.34% vs. 7.62 ± 6.50%, $p = 0.045$). There were no significant differences between benign and malignant lesions in TTP ($p = 0.52$) or AUC ($p = 0.06$). Additionally, the two-parameter exponential recovery model did not yield any significant differences between benign and malignant masses for any of the three parameters ($p = 0.72$ for α; $p = 0.19$ for β; and $p = 0.07$ for $\alpha \times \beta$).

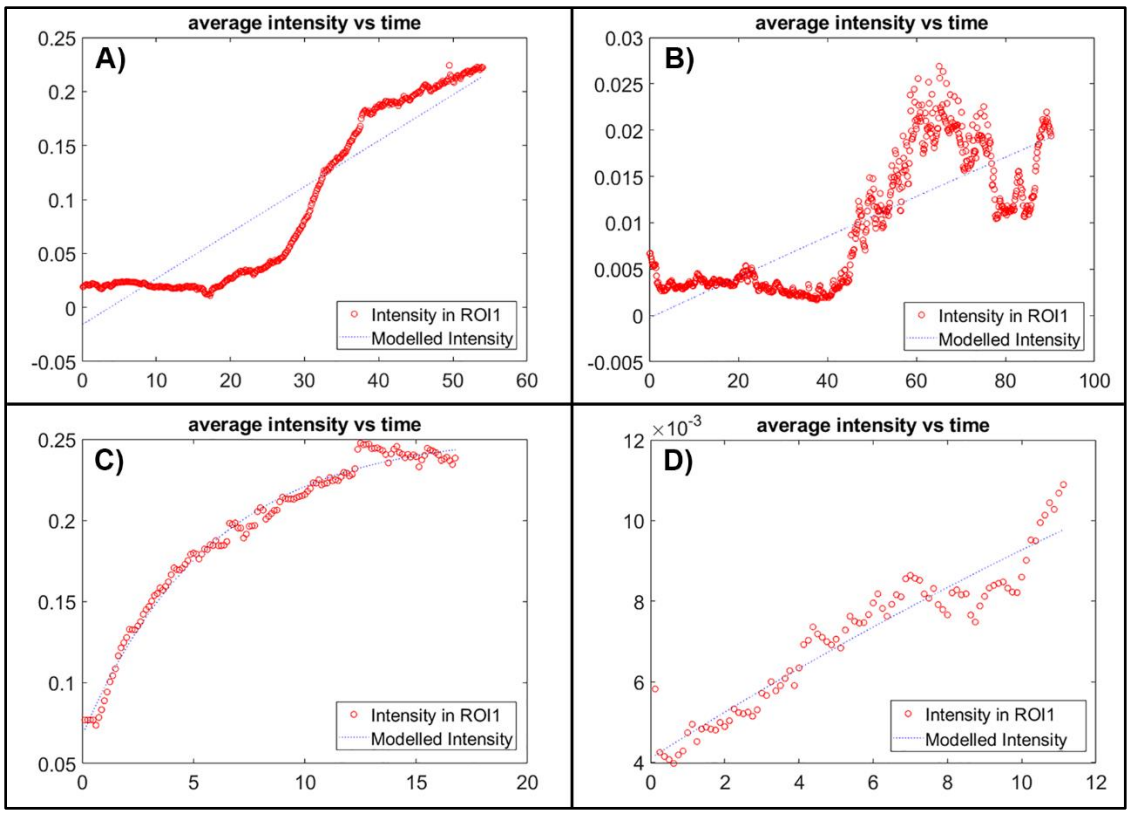

Figure 2: Representative time-intensity curves from study patients. A) Initial wash-in of contrast within a lesion later classified as malignant by pathology. B) Initial wash-in of contrast within a lesion later classified as benign by pathology. C) A representative flash-replenishment sequence from the malignant lesion shown in A. D) A representative flash-replenishment sequence from the benign lesion shown in B. ***NOTE: The y-axis values are scaled to the data in each curve for better visualization.***

Diagnostic accuracy was calculated for each SHI parameter. The fraction of the lesion showing perfusion had the highest diagnostic accuracy at 81%. The rest of the parameters ranged in accuracy from 52% (TTP) to 79% (model parameter α). All diagnostic accuracies are presented in Table 1.

Radiological Scoring of CEUS and SHI Clips

The performance of the radiologists on the qualitative assessment of the contrast-enhanced SHI clips demonstrates the importance of familiarity and experience with CEUS. The diagnostic confidence of the experienced radiologist significantly increased when reviewing the SHI imaging (86 ± 28%) compared to grayscale only (68 ± 23%, p = 0.042). There was no change in the diagnostic confidence for the novice radiologist between SHI (86 ± 15%) and grayscale (83 ± 15%, p = 0.27). The ROC curves associated with pre- and post-contrast diagnostic confidence for both radiologists are shown in Figure 3.

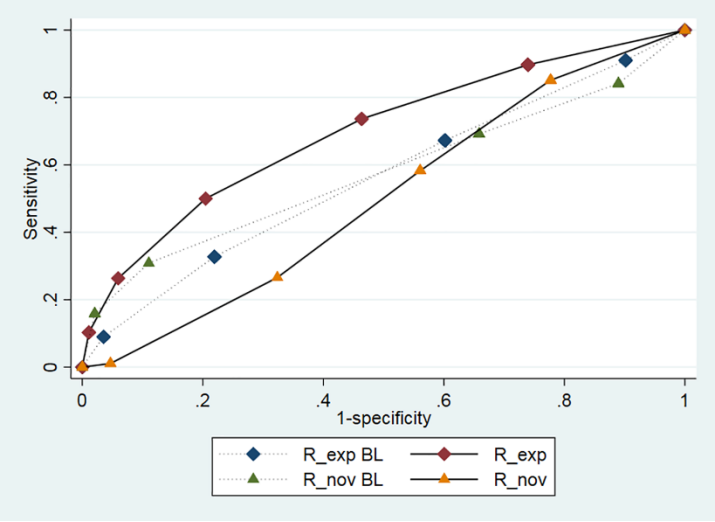

Figure 3: ROC curves for diagnostic confidence for both novice (R_nov) and experienced (R_exp) radiologists before (BL for baseline) and after contrast-enhanced SHI.

There was also no difference in diagnostic confidence between the experienced and novice radiologists when reviewing the SHI clips (p = 0.50). Additionally, as shown in

Figure 4, qualitative analysis of the SHI images by the experienced radiologist resulted in a diagnostic accuracy of 70%, compared to 56% without contrast, while the novice radiologist only saw a 7% improvement (from 50% to 58%, Fig. 4A). When the radiologist reads are combined with the most predictive quantitative SHI parameter (% perfusion; PER), diagnostic accuracy improved to 84% for the experienced radiologist and 96% for the novice radiologist (Fig. 4B); this difference was not significant (p = 0.32). However, given that both radiologists saw improvement in diagnostic accuracy once the quantitative parameter (PER) was included in the ROC model, these results suggest that the PER parameter adds diagnostic value.

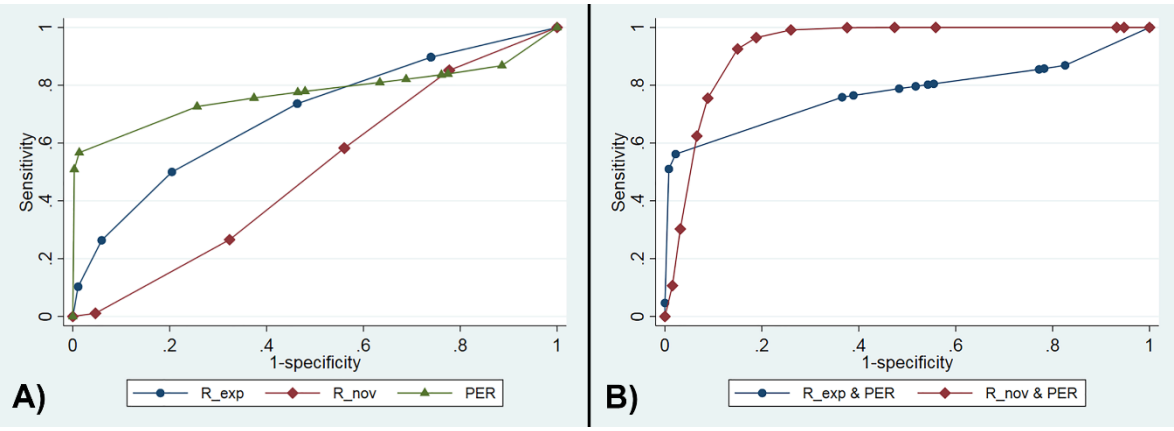

Figure 4: ROC curves of diagnostic data. A) Analysis of the experienced radiologist (R_{exp}), novice radiologist (R_{nov}), and highest quantitative SHI parameter (perfusion %, PER). B) Combination of PER with radiologist reads.

Discussion

Only 10-20% of all ovarian lesions surgically excised are malignant [53], highlighting the necessity for a more definitive pre-operative classification via imaging.

Such a modality could increase the pre-operative confidence for differentiating benign from malignant lesions, therefore diminishing the number of indeterminate lesions that necessitate surgery for classification.

This work represents, to our knowledge, the first study to investigate the use of endovaginal contrast-enhanced SHI imaging in women scheduled to undergo surgery for an adnexal mass as a potential tool for characterizing the malignancy of the lesion. We demonstrated that contrast-enhanced SHI imaging, particularly the quantitative parameters derived from subharmonic time-intensity curves, could achieve diagnostic accuracies up to 81%. Additionally, the diagnostic accuracy of the experienced radiologist improved by 14% with the addition of contrast-enhanced SHI imaging, suggesting that it is a valuable tool for clinical adaptation; albeit in a small sample size. Our findings suggest that noninvasive, endovaginal, contrast-enhanced SHI imaging may become a clinical imaging modality for evaluating adnexal masses with the potential to reduce both cost and risk to the patient, while also improving diagnostic accuracies. In this study, we specifically evaluated SHI imaging. It is conceivable that replacing or combining SHI with other tissue suppression methods, such as amplitude modulation (similar to CPS) or pulse inversion, would improve results further. However, establishing this will require further experiments.

Quantitative analysis of the contrast-enhanced SHI images showed that malignant adnexal masses had a significantly greater perfusion than those classified as benign. We expected that malignant tumors would demonstrate tumor angiogenesis and increased blood flow [16, 17, 19], and our findings that this is identifiable with endovaginal contrast-enhanced SHI is supported by other studies using CEUS imaging [15, 29].

We also found that clinical screening factors for malignancy were inconclusive in distinguishing benign from malignant masses in our limited study population; however, there was large deviation in the malignant group. CA-125 levels are only clinically relevant for later stage ovarian cancer, as this serum marker lacks sensitivity in early stage disease [54, 55]. One patient with a malignant mass presented with a CA-125 level of 143 U/mL, was staged as IIB high-grade serous ovarian cancer, and is now in remission, while another patient with malignancy presented with a CA-125 level of 12.8 U/mL and has since succumbed to disease. However, the average CA-125 level for patients with benign lesions was 19.3 U/mL, with only one patient below the 12.8 U/mL observed for a patient with malignancy. These cases highlight the insufficiency of CA-125 as a predictor for malignancy in ovarian masses.

RMI is calculated from CA-125, as well as patient age, menopausal status, and clinical impression [56], so inherently a lack of difference in CA-125 levels between the two pathological classifications would suggest that RMI would also be similar. We suspect that differences in CA-125 and RMI would appear between malignant and benign masses with increased sample sizes, as comparing 3 malignant lesions versus 5 benign lesions is hardly an ideal comparison. However, we did find that RMI had a higher diagnostic accuracy at 73% than CA-125 levels alone (60%), suggesting that the other factors used in calculating the RMI score (including an ultrasound score) [55, 56] provide a better overall assessment of the lesion. Given the high diagnostic accuracy provided by contrast-enhanced SHI, this modality could possibly be incorporated into the RMI calculation in the future, providing an even better ultrasound score and potentially further improving clinical classification of adnexal masses based on this modified RMI.

One limitation to this pilot study is the small sample size, with only ten patients completing the study at a single medical center. Therefore, we cannot definitely determine whether the observed differences between benign and malignant adnexal masses, as measured with contrast-enhanced SHI, can serve as an effective diagnostic tool. However, it is encouraging that all of the significant findings support this trend. Further investigation, with larger sample sizes at multiple centers, is necessary to determine whether contrast-enhanced SHI evaluation of adnexal masses could be a noninvasive, real-time, quantitative factor for determining malignancy and the need for surgical intervention (at least in high-risk populations [53]). Also, although *in vitro* and animal *in vivo* studies show that other UCAs are also effective in intermittent destruction-replenishment CEUS perfusion imaging [57, 58], we limited our pilot study to only use Definity contrast agent. Definity represents one of only three UCAs that are commercially available and FDA approved for use in humans in echocardiography, and we have previously had success with off-label use of Definity [25, 40, 59].

The potential clinical impact of these findings is promising, as there is no definitive noninvasive method for determining malignancy in ovarian lesions. Coupled with clinical standard of care evaluations, contrast-enhanced SHI for pre-surgical characterization of ovarian masses may improve the determination of malignancy, reducing cost and risk to patients, while improving diagnostic accuracy; albeit based on a small sample size.

Acknowledgements

The authors would like to thank Dr. Jaimie Dougherty from Drexel University for her contributions to this work. We also thank GE Healthcare for equipment support and

Lantheus Medical Imaging for providing Definity. This work was supported by NIH grants R21 CA190930 and F32 AR072491.

Figure Captions List

Figure 1: Representative SHI images from study patients. A) Pre-contrast image of a lesion later classified as malignant by pathology. B) Pre-contrast image of a lesion later classified as benign by pathology. C) SHI of the malignant lesion shown in panel A. D) SHI of the benign lesion shown in panel B.

Figure 2: Representative time-intensity curves from study patients. A) Initial wash-in of contrast within a lesion later classified as malignant by pathology. B) Initial wash-in of contrast within a lesion later classified as benign by pathology. C) A representative flash-replenishment sequence from the malignant lesion shown in A. D) A representative flash-replenishment sequence from the benign lesion shown in B. ***NOTE: The y-axis values are scaled to the data in each curve for better visualization.***

Figure 3: ROC curves for diagnostic confidence for both novice (R_nov) and experienced (R_exp) radiologists before (BL for baseline) and after contrast-enhanced SHI.

Figure 4: ROC curves of diagnostic data. A) Analysis of the experienced radiologist (R_{exp}), novice radiologist (R_{nov}), and highest quantitative SHI parameter (perfusion %, PER). B) Combination of PER with radiologist reads.

Tables

*Table 1: Summary of quantitative SHI analysis. *p = 0.046, **p = 0.045, ^ most predictive quantitative SHI parameter.*

	Time to Peak Contrast, **TTP** (s)	Peak Contrast Intensity, **PI** (AU)	Fraction of Lesion with Perfusion, **PER** (%)	Area Under the Curve, **AUC** (AU)	Model **α**, correlative μvessel cross-sectional area (dB)	Model **β**, Blood Velocity (mm/s)	Model **α x β**, Perfusion per Tissue (mL/s*mg)
Benign (n=8)	142.79 ± 122.26	0.05 ± 0.03*	7.62 ± 6.50**	0.72 ± 0.50	0.76 ± 1.97	0.10 ± 0.07	$5.84 \times 10^{-3} \pm 5.73 \times 10^{-3}$
Malignant (n = 4)	140.35 ± 22.45	0.11 ± 0.09*	24.79 ± 25.34**	1.61 ± 1.30	0.16 ± 0.06	0.14 ± 0.08	$1.89 \times 10^{-2} \pm 2.19 \times 10^{-2}$
Diagnostic Accuracy (A_z)	52%	72%	81%^	75%	79%	71%	75%

References

1. Ferlay, J., et al., *Cancer incidence and mortality worldwide, international agency for research on cancer.* Cancer incidence and mortality worldwide, International agency for research on cancer, 2013: p. 120-63.
2. Torre, L.A., et al., *Ovarian cancer statistics, 2018.* CA: a cancer journal for clinicians, 2018. **68**(4): p. 284-296.
3. Mitchell, D.G., et al., *ACR Appropriateness Criteria Staging and Follow-up of Ovarian Cancer.* Journal of the American College of Radiology, 2013. **10**(11): p. 822-827.
4. Jinawath, N. and I.M. Shih, *Biology and Pathology of Ovarian Cancer*, in *Early Diagnosis and Treatment of Cancer Series: Ovarian Cancer*, R. Briston and D. Armstrong, Editors. 2011, Saunders: Philadelphia, PA. p. 17-32.
5. Siegel, R.L., K.D. Miller, and A. Jemal, *Cancer statistics, 2018.* CA: A Cancer Journal for Clinicians, 2018. **68**(1): p. 7-30.
6. Mohaghegh, P. and A.G. Rockall, *Imaging strategy for early ovarian cancer: characterization of adnexal masses with conventional and advanced imaging techniques.* Radiographics, 2012. **32**(6): p. 1751-1773.
7. Moyle, P., H.C. Addley, and E. Sala. *Radiological staging of ovarian carcinoma*. in *Seminars in Ultrasound, CT and MRI*. 2010. Elsevier.
8. Fishman, D.A., et al., *The role of ultrasound evaluation in the detection of early-stage epithelial ovarian cancer.* American Journal of Obstetrics & Gynecology, 2005. **192**(4): p. 1214-1221.

9. Hricak, H., et al., *Complex Adnexal Masses: Detection and Characterization with MR Imaging—Multivariate Analysis.* Radiology, 2000. **214**(1): p. 39-46.
10. Spencer, J.A., et al., *ESUR guidelines for MR imaging of the sonographically indeterminate adnexal mass: an algorithmic approach.* European Radiology, 2010. **20**(1): p. 25-35.
11. Curtin, J.P., *Management of the Adnexal Mass.* Gynecologic Oncology, 1994. **55**(3): p. S42-S46.
12. Narasimhulu, D.M., F. Khoury-Collado, and D.S. Chi, *Radical Surgery in Ovarian Cancer.* Current Oncology Reports, 2015. **17**(4): p. 16.
13. Eskander, R., M. Berman, and L. Keder, *Practice Bulletin No. 174: Evaluation and Management of Adnexal Masses.* Obstetrics & Gynecology, 2016. **128**(5).
14. Fleischer, A.C., *Early Detection of Ovarian Cancer with Transvaginal Microbubble Sonography: Current and Potential Applications.* Gynecol Obstet (Sunnyvale), 2017. **7**(06): p. 2161-0932.
15. Szymanski, M., et al., *Differentiating between benign and malignant adnexal lesions with contrast-enhanced transvaginal ultrasonography.* International Journal of Gynecology & Obstetrics, 2015. **131**(2): p. 147-151.
16. Folkman, J., *What Is the Evidence That Tumors Are Angiogenesis Dependent?* JNCI: Journal of the National Cancer Institute, 1990. **82**(1): p. 4-7.
17. Li, W.W., *Tumor angiogenesis: molecular pathology, therapeutic targeting, and imaging.* Academic radiology, 2000. **7**(10): p. 800-811.

18. Brawer, M.K., S.A. Bigler, and R.E. Deering, *Quantitative morphometric analysis of the microcirculation in prostate carcinoma.* Journal of Cellular Biochemistry, 1992. **50**(S16H): p. 62-64.
19. Weidner, N., et al., *Tumor angiogenesis and metastasis—correlation in invasive breast carcinoma.* New England Journal of Medicine, 1991. **324**(1): p. 1-8.
20. Labiche, A., et al., *Prognostic significance of tumour vascularisation on survival of patients with advanced ovarian carcinoma.* Histology and histopathology, 2009. **24**(4): p. 425.
21. Palmer, J.E., et al., *Prognostic value of measurements of angiogenesis in serous carcinoma of the ovary.* International Journal of Gynecological Pathology, 2007. **26**(4): p. 395-403.
22. Jain, R.K., *Barriers to drug delivery in solid tumors.* Scientific American, 1994. **271**(1): p. 58-65.
23. Bazot, M., et al., *Value of magnetic resonance imaging for the diagnosis of ovarian tumors: a review.* Journal of computer assisted tomography, 2008. **32**(5): p. 712-723.
24. Goldberg, B.B., J.S. Raichlen, and F. Forsberg, *Ultrasound contrast agents: basic principles and clinical applications*. 2001: Informa Healthcare.
25. Sridharan, A., et al., *Perfusion estimation using contrast enhanced three-dimensional subharmonic ultrasound imaging: an in vivo study.* Investigative radiology, 2013. **48**(9): p. 654.

26. Fleischer, A.C., et al., *Advances in sonographic detection of ovarian cancer: depiction of tumor neovascularity with microbubbles.* American Journal of Roentgenology, 2010. **194**(2): p. 343-348.
27. Wang, J., et al., *Study on the characteristics of contrast-enhanced ultrasound and its utility in assessing the microvessel density in ovarian tumors or tumor-like lesions.* International journal of biological sciences, 2011. **7**(5): p. 600.
28. Testa, A.C., et al., *The use of contrasted transvaginal sonography in the diagnosis of gynecologic diseases: a preliminary study.* Journal of ultrasound in medicine, 2005. **24**(9): p. 1267-1278.
29. Marret, H., et al., *Contrast-enhanced sonography helps in discrimination of benign from malignant adnexal masses.* Journal of ultrasound in medicine, 2004. **23**(12): p. 1629-1639.
30. Ordén, M.-R., J.S. Jurvelin, and P.P. Kirkinen, *Kinetics of a US contrast agent in benign and malignant adnexal tumors.* Radiology, 2003. **226**(2): p. 405-410.
31. Hamilton, M.F. and D.T. Blackstock, *Nonlinear acoustics*. Vol. 237. 1998: Academic press San Diego.
32. Forsberg, F., W.T. Shi, and B.B. Goldberg, *Subharmonic imaging of contrast agents.* Ultrasonics, 2000. **38**(1-8): p. 93-98.
33. Shankar, P.M., P.D. Krishna, and V.L. Newhouse, *Advantages of subharmonic over second harmonic backscatter for contrast-to-tissue echo enhancement.* Ultrasound in medicine & biology, 1998. **24**(3): p. 395-399.
34. Dave, J.K., et al., *Static and dynamic cumulative maximum intensity display mode for subharmonic breast imaging: a comparative study with mammographic*

and conventional ultrasound techniques. Journal of Ultrasound in Medicine, 2010. **29**(8): p. 1177-1185.

35. Dave, J.K., et al., *Noninvasive estimation of dynamic pressures in vitro and in vivo using the subharmonic response from microbubbles.* IEEE transactions on ultrasonics, ferroelectrics, and frequency control, 2011. **58**(10): p. 2056-2066.
36. Dave, J.K., et al., *Processing of subharmonic signals from ultrasound contrast agents to determine ambient pressures.* Ultrasonic imaging, 2012. **34**(2): p. 81-92.
37. Bhagavatheeshwaran, G., et al., *Subharmonic signal generation from contrast agents in simulated neovessels.* Ultrasound in medicine & biology, 2004. **30**(2): p. 199-203.
38. Dave, J.K. and F. Forsberg, *Novel automated motion compensation technique for producing cumulative maximum intensity subharmonic images.* Ultrasound in medicine & biology, 2009. **35**(9): p. 1555-1563.
39. Eisenbrey, J.R., et al., *Simultaneous grayscale and subharmonic ultrasound imaging on a modified commercial scanner.* Ultrasonics, 2011. **51**(8): p. 890-897.
40. Eisenbrey, J.R., et al., *Parametric imaging using subharmonic signals from ultrasound contrast agents in patients with breast lesions.* Journal of Ultrasound in Medicine, 2011. **30**(1): p. 85-92.
41. Eisenbrey, J.R., et al., *Assessing algorithms for defining vascular architecture in subharmonic images of breast lesions.* Physics in Medicine & Biology, 2011. **56**(4): p. 919.

42. Forsberg, F., et al., *Breast lesions: imaging with contrast-enhanced subharmonic US—initial experience.* Radiology, 2007. **244**(3): p. 718-726.
43. Chomas, J., et al., *Nondestructive subharmonic imaging.* IEEE transactions on ultrasonics, ferroelectrics, and frequency control, 2002. **49**(7): p. 883-892.
44. Faez, T., et al., *Characterizing the subharmonic response of phospholipid-coated microbubbles for carotid imaging.* Ultrasound in medicine & biology, 2011. **37**(6): p. 958-970.
45. Faez, T., et al., *Dynamic manipulation of the subharmonic scattering of phospholipid-coated microbubbles.* Physics in Medicine & Biology, 2011. **56**(19): p. 6459.
46. Goertz, D.E., et al., *Subharmonic contrast intravascular ultrasound for vasa vasorum imaging.* Ultrasound in medicine & biology, 2007. **33**(12): p. 1859-1872.
47. Helfield, B.L., et al., *Investigating the subharmonic response of individual phospholipid encapsulated microbubbles at high frequencies: A comparative study of five agents.* Ultrasound in medicine & biology, 2012. **38**(5): p. 846-863.
48. Misaridis, T.X., et al., *Potential of coded excitation in medical ultrasound imaging.* (0041-624X (Print)).
49. Krix, M., et al., *A multivessel model describing replenishment kinetics of ultrasound contrast agent for quantification of tissue perfusion.* Ultrasound in Medicine & Biology, 2003. **29**(10): p. 1421-1430.
50. Krix, M., et al., *Quantification of perfusion of liver tissue and metastases using a multivessel model for replenishment kinetics of ultrasound contrast agents.* Ultrasound in Medicine & Biology, 2004. **30**(10): p. 1355-1363.

51. Wei, K., et al., *Quantification of myocardial blood flow with ultrasound-induced destruction of microbubbles administered as a constant venous infusion.* Circulation, 1998. **97**(5): p. 473-483.
52. Metz, C.E., *ROC methodology in radiologic imaging.* (0020-9996 (Print)).
53. Ross, E.K. and M. Kebria, *Incidental ovarian cysts: When to reassure, when to reassess, when to refer.* Cleveland clinic journal of medicine, 2013. **80**(8): p. 503-514.
54. Duffy, M.J., et al., *CA125 in ovarian cancer: European Group on Tumor Markers guidelines for clinical use.* International Journal of Gynecological Cancer, 2005. **15**(5): p. 679-691.
55. Karlsen, M.A., et al., *Evaluation of HE4, CA125, risk of ovarian malignancy algorithm (ROMA) and risk of malignancy index (RMI) as diagnostic tools of epithelial ovarian cancer in patients with a pelvic mass.* Gynecologic oncology, 2012. **127**(2): p. 379-383.
56. Jacobs, I., et al., *A risk of malignancy index incorporating CA 125, ultrasound and menopausal status for the accurate preoperative diagnosis of ovarian cancer.* BJOG: An International Journal of Obstetrics & Gynaecology, 1990. **97**(10): p. 922-929.
57. Moran, C.M., et al., *Quantification of microbubble destruction of three fluorocarbon-filled ultrasonic contrast agents.* Ultrasound in medicine & biology, 2000. **26**(4): p. 629-639.
58. Seol, S.-H., et al., *Real-time contrast ultrasound muscle perfusion imaging with intermediate-power imaging coupled with acoustically durable microbubbles.*

Journal of the American Society of Echocardiography, 2015. **28**(6): p. 718-726. e2.

59. Linden Robert, A., et al., *Contrast Enhanced Ultrasound Flash Replenishment Method for Directed Prostate Biopsies.* Journal of Urology, 2007. **178**(6): p. 2354-2358.